FLOW ARRANGEMENT AND HEAT TRANSFER CAPABILITIES OF A PLASMA FACING COMPONENT IN THE FORM OF A CPS

L. Th. Benos[1] and N. A. Pelekasis[2]

[1,2]Department of Mechanical Engineering, University of Thessaly

Volos, GR-38334, Greece
e-mail: [1]ebenos@uth.gr, [2]pel@uth.gr

Keywords: PFCs, CPS, static configuration, capillary motion, finite element method.

Abstract. *Free surface plasma facing components constitutes one of the most critical technological studies in order to circumvent problems pertaining to the plasma-wall interaction. The flow pattern of liquid metals employed for protection of the divertor region and the blanket first wall is characterized by the formation of a free surface that is subjected to strong electromagnetic fields and heat load generated by the plasma. This study investigates the static configuration of the Capillary Porous System, taking into consideration the capillary force, the effect of an external electric field and the dielectric constants of the two media. Thus, the shape of the liquid metal "drop" resting upon the wafer is derived numerically using the finite element method. Furthermore, the capillary rise in a single pore is studied for a fluid resting in a reservoir of fixed pressure, in order to demonstrate the basic concept in the operation of the CPS as a capillary pump. The finite element method is employed in order to capture the time evolution of the interface accounting for viscous, inertia and static pressure resistance to motion. The effect of pore size and material properties on the rise velocity is investigated.*

1 INTRODUCTION

Free surface plasma facing components (PFCs) are of great importance concerning future fusion reactors since they should have the ability to withstand power densities of the order 5-10 MW/m^2 and up to 100 MW/m^2 for off-normal events such as edge-localized modes (ELM's) and disruptions. The plasma-wall interaction that is generated by such events is expected to cause problems such as erosion, thermal stresses, thermal fatigue and tritium retention which are difficult to deal with. In order to circumvent the above problems liquid metals are considered as alternative plasma facing components [1]. The self-cooling and self-annealing properties of flowing liquids increase their life cycle as they interact with the core plasma of the fusion reactor. The liquid metal can be supplied in the form of (a) a free flowing liquid metal sheet or a jet-drop curtain [2], (b) a continuously flowing film that coats the divertor wall [3] or (c) a capillary porous system [4] that contains the liquid metal by capillarity and controls the replenishment of the liquid metal in contact with plasma.

Preliminary experimental studies with liquid lithium as the operating fluid provide encouraging results [2-5] in terms of power exhaust and plasma contamination, while revealed the potential for a positive impact of lithium in the deuterium/tritium inventory. As an alternative to lithium, liquid gallium has also been considered as PFC, due to its low reactivity and much wider liquid state temperature range. The concepts of a jet-drop curtain and liquid metal sheet were among the first to be tested as a means to assist power exhaust from fusion reactors. In both cases [5-7] hydrodynamic instability was seen to destabilize the liquid metal carrier, thus generating liquid metal drops which were then observed to be deflected towards the reactor walls as a result of *JxB* effects. A recent first-principle study [8] verified the strong deflection of a gallium drop as a result of the interaction between the electric and magnetic fields that surround it.

The concept of a flowing film that coats the divertor walls has also been investigated [9] with emphasis placed in the thin wall configuration, convective liquid flow first wall (CLIFF), concept. However the necessary speed and thickness of the film that coats the reactor walls are such that hydrodynamic instabilities may set in as soon as the film exits the inlet nozzle. As a result the flow arrangement will soon lose its coherence and fail to protect the reactor walls from the oncoming heat load from the reactor core.

The suggestion of using surface tension forces for suppression of lithium splashing was based on the idea of compensation of ponder motive forces in liquid metals by surface tension forces in the interior of a porous matrix that rests upon the divertor area and provides contact with the plasma interior. These porous matrices made from Mo, stainless steel (SS), V or W are manufactured as pressed wire grids and are called "capillary-pore systems' (CPS). Two micrograph photos of typical CPS from 100μm Mo-grids with, fig. 1a, and without, fig. 1b, Li filling are presented in Figure 1.

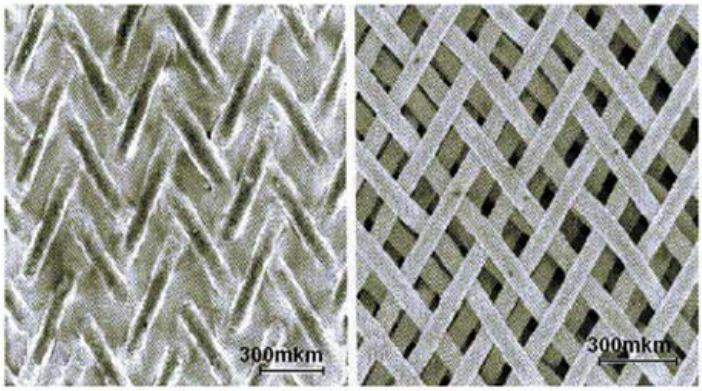

(a) (b)

Figure 1. View of the 100μm CPS with (a) and without (b) Li filling (top) [4]

Modelling of the power exhaust capabilities of such a system requires knowledge of the flow arrangement, if at all present. The extent of convective heat transfer required for proper interception of the heat load and the resulting evaporation rate are central issues. Thus far, the capillary porous system (CPS) has not been the subject of extensive modelling activity partly due to the complex flow arrangement of the limiter containing the liquid metal. Available studies [4,10,11] focus on the importance of the capillary forces to supply a mass flow rate of lithium through the CPS system via a qualitative balance between capillary pressure and the different resistances to flow. Based on the geometry of the existing CPS configurations, assuming a static configuration in the CPS system that is in contact with a reservoir at 200^{o}C while facing a heat load on the order of several MW's, e.g. ~10MW/m^2, would amount to a temperature gradient on the order of 300^{o}C across a pore matrix that is 1 mm thick with an average thermal conductivity on the order of 30 W/(m K). As the heat load approaches the threshold value of 20MW/m^2, based on estimates obtained from observations of divertor degradation at the JET facility, either unrealistically large temperature gradients are obtained, on the order of 700^{o}C, in the absence of any appreciable liquid metal evaporation, or exceedingly large evaporation rates will arise, if the interface between plasma and liquid metal is to maintained at a relatively low temperature, <1000^{o}C. In the former case, large interfacial temperatures may induce hydrogen combustion as a side effect of liquid lithium reaction in a fusion reactor [12]. However, this would require quite large temperatures, >1000^{o}C, in order for hydrogen retention in the form of LiH to be arrested. On the other hand, large evaporation rates would lead to plasma contamination via lithium vapor diffusion through the surrounding e-layer [1]. Clearly then, large heat loads will lead to large evaporation rates or large temperature levels at the interface with plasma, followed by depletion of the liquid metal layer covering the CPS system. Consequently, efficient replenishment of the interface with plasma is required for reliable operation of the CPS system to be achieved. This is provided by flow in the small capillaries of the matrix that serves to supply liquid lithium to the top of the porous matrix at a speed that depends on the pressure difference between the lithium reservoir and the plasma interface, pore size and material properties.

A study of the above described action of the porous matrix as a capillary pump is performed in the present study, focusing on the factors affecting lithium transport through a micropore of the CPS. A fixed pressure drop between the liquid metal reservoir and the external medium is assumed and its relative importance in comparison with capillary pressure is assessed depending primarily on the pore size. To this end the finite element methodology is employed for the numerical solution of the shape and speed of the liquid metal column that is generated inside each micropore of the CPS as soon as a region of depleted liquid lithium arises on the exterior surface. Static, viscous and inertia resistance to motion is taken into account. As a first step a quasi-steady state flow arrangement is considered with the velocity profile in the pore immediately adjusting once the shape of the interface is established.

2 INVESTIGATION OF STATIC ARRANGEMENT

2.1 Modeling and mathematical formulation

As a first approach, the static configuration of the liquid coolant is examined as it rests on top of the CPS in contact with plasma. The entire arrangement follows the CPS matrix employed at Frascati [13], fig. 2a. The entire top surface of the CPS structure is assumed to be covered by a liquid metal which is pinned onto the rim of the surface, fig. 2b. The pressure inside the CPS is unknown and will be determined upon calculation of the

drop shape. Both the hydrostatic and an approximate hydro-electro-static cases are considered using axially symmetric models. In the latter case, the liquid metal is placed inside the reactor chamber treated as a capacitor that prescribes an external electric field. The Young-Laplace equation at the interface and the integral force balance over the entire "drop" surface resting upon the CPS wafer, determine the static configuration using a known contact angle. Both media are treated as perfect dielectrics while the "drop" thickness is taken to be small with respect to its length in order to estimate the electric stresses.

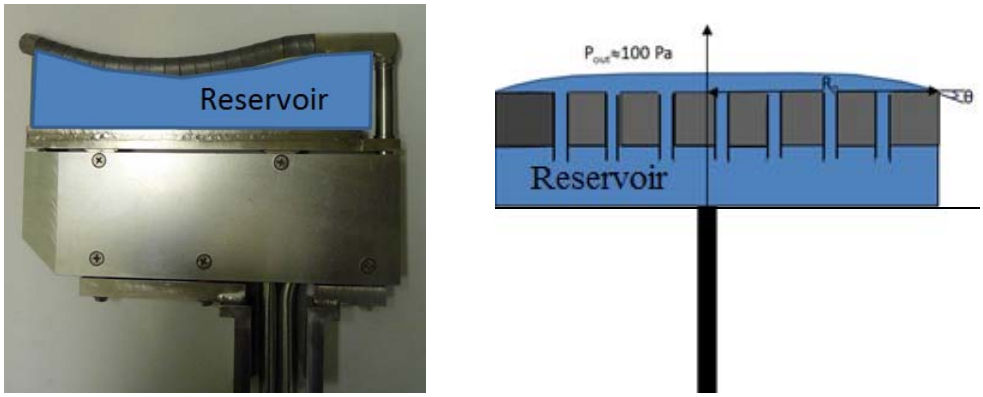

(a) (b)

Figure 2: (a) Frascati CPS matrix and (b) Schematic diagram of the static configuration

At static equilibrium, fig. 2b, the Young-Laplace equation holds at the liquid metal plasma interface where surface tension balances pressure drop and electric stresses that arise as a result of the different electric permittivities of the two media [14], i.e. liquid metal and plasma:

$$\mathbf{n}\left(P_{in}-P_{out}\right)\underline{\underline{I}}+\mathbf{n}\left(\underline{\underline{\tau_e^{out}}}-\underline{\underline{\tau_e^{in}}}\right)+\mathbf{n}2H\sigma=0 \tag{1}$$

In addition, the integral force balance for the entire "drop" resting on the wafer surface reads:

$$\int_0^{2\pi}\int_0^{R_c}\left(P_{in}-\rho g h_0-P_{out}\right)rdrd\theta-\int_0^{2\pi}\int_0^{R_c}\rho gzrdrd\theta-2\pi\sigma R_c\sin\theta+\int_0^{2\pi}\int_0^{R_c}\left(\underline{\underline{\tau_e^{out}}}-\underline{\underline{\tau_e^{in}}}\right)rdrd\theta=0 \tag{2}$$

where θ is the contact angle, h_0 is the CPS height, g is the gravitational acceleration, **n** is the normal to the interface unit vector, P_{in}, P_{out} are the pressures in the liquid metal and the surrounding plasma, respectively, ρ, σ are the liquid metal density and its surface tension, respectively, $\underline{\underline{I}}$ denotes the unit tensor while $\underline{\underline{\tau_e^{in}}}$ and $\underline{\underline{\tau_e^{out}}}$ stand for the electric stress tensors of liquid metal and plasma, respectively, whose difference is given by the following relation:

$$\mathbf{n}\cdot\left(\underline{\underline{\tau_e^{out}}}-\underline{\underline{\tau_e^{in}}}\right)=\mathbf{n}\frac{\varepsilon_{out}\left(1-\varepsilon_{out}/\varepsilon_{in}\right)}{2}\left(\frac{\partial\Phi}{\partial n}^2+\frac{\varepsilon_{in}}{\varepsilon_{out}}\frac{\partial\Phi}{\partial s}^2\right) \tag{3}$$

where ε_{in}, ε_{out} denote the electric permittivities of liquid metal and plasma, respectively

When an external electric field is applied, taking the "drop" to be thin, $z/R_c<<1$, the boundary conditions for the electric potential at the interface simplify as follows:

$$\frac{\partial\Phi}{\partial n}\approx\frac{d\Phi}{dz}=a,\quad \frac{\partial\Phi}{\partial s}\approx\frac{d\Phi}{dz}\frac{dz}{ds}\rightarrow\mathbf{n}\cdot\left(\underline{\underline{\tau_e^{out}}}-\underline{\underline{\tau_e^{in}}}\right)\equiv\mathbf{n}\,\tau_{el}\approx\mathbf{n}\frac{a^2\varepsilon_{out}\left(1-\varepsilon_{out}/\varepsilon_{in}\right)}{2\left(1+z_r^2\right)}\left[1+\frac{\varepsilon_{in}}{\varepsilon_{out}}z_r^2\right] \tag{4}$$

The above assumption loses validity in the vicinity of the of the drop equator where the normal potential gradient $\partial\Phi/\partial n$ is much smaller than its value at the pole, a. For comparable film thickness and length the

boundary element method may be used to calculate the electric potential inside and outside the film [14,15] more accurately.

2.2 Main results

The governing forces applied on the liquid metal drop are clearly depicted in Figure 3. Capillary forces are important at the contact line of the liquid metal drop covering the CPS provided there is a contact region between the liquid metal, the CPS and the surrounding plasma. The goal of the study is to obtain the drop shape and interior pressure for given radius of the CPS matrix. Alternatively the extent of liquid metal coverage on top of the CPS system can be obtained for fixed pressure drop between the liquid metal reservoir and the surrounding medium. The aforementioned problem formulation was solved with the finite element methodology assuming axisymmetry and using the physical and thermophysical properties of lithium provided in [10].

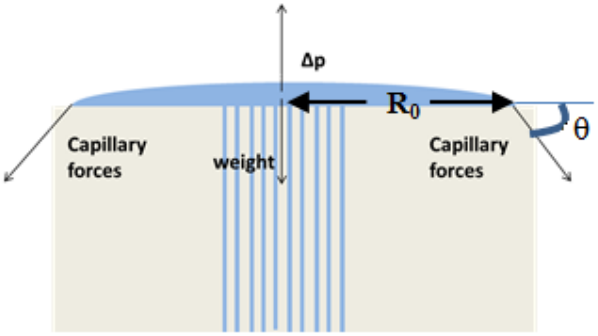

Figure 3. Dominant forces applied on the "drop"

As the drop size decreases, gravity does not play such an important role (microfluidic regime). Consequently, as the pressure drop between the reservoir and the surrounding medium increases the drop does not extend significantly and the dominant force balance is between pressure drop and capillarity:

$$\Delta p \pi R_c^2 \sim 2\pi R_c \sigma \sin\theta \tag{5}$$

As pressure drop decreases, while gravity still remains out of the picture, the dominant balance leads to a larger spread radius, as can be seen in Figure 4. As the drop further spreads out the importance of gravity increases until it becomes dominant, to the point that a static balance is not possible anymore. This result holds whether the study fixes the drop radius and solves for the shape and internal pressure, as is more relevant to the prevailing arrangement of CPS systems in existing machines, or by fixing the pressure drop between the reservoir and the surrounding medium while looking for the extent of drop coverage on the CPS top surface.

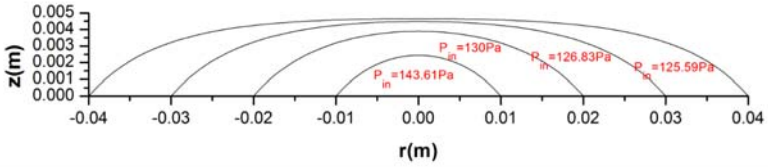

Figure 4. Drop shape and internal pressure for different size of the porous structure

Upon introduction of electric stresses in the normal force balance due to an external electric field, the effective internal pressure is affected thus rearranging the extent of the drop. This is better illustrated when $\varepsilon_{out}/\varepsilon_{in}<<1$, Figure 5, in which case a perfectly conducting liquid metal is assumed [14,15] while the formulation of the electrostatic problem assumes the form,

$$\partial\Phi/\partial s|_{in} = 0, \Phi_{in} = 0, \vec{\nabla}\Phi\left(\vec{r}\to\infty\right) = az, \nabla^2\Phi = 0, \quad \tau_{el} = \frac{\varepsilon_{out}}{2}\left(\partial\Phi/\partial n|_{out}\right)^2 \approx \frac{\varepsilon_{out}}{2}\frac{a^2}{1+z_r^2} \tag{6}$$

Increasing the external electric field intensity, dΦ/dz=a, the drop size decreases since the internal pressure increases as well. In this case increasing the external electric field amounts to increasing the effective internal

pressure. This forces material out of the CPS matrix at static equilibrium thus reducing its size. It should be stressed that when a different configuration is adopted, i.e. that of a conducting drop that freely elongates in response to an increasing electric field [16], where drop adhesion onto a solid substrate (the CPS system in our case) is not present, the electric field may eventually destroy the drop releasing liquid jets consisting of its interior liquid metal.

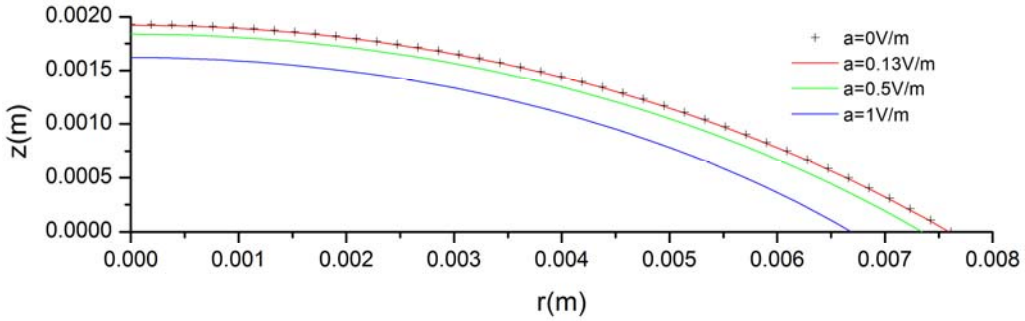

Figure 5. Drop shape with increasing electric field intensity for Δp=80 Pa and $\varepsilon_{out}/\varepsilon_{in}$=1/100

In a nutshell, the increment of the pressure drop, the electric field and the ratio of electric permittivities $\varepsilon_{out}/\varepsilon_{in}$ contribute to the shrinking of the liquid metal drop which rests on top of the porous matrix. When the dynamic flow configuration is considered, on the other hand, any additional normal pressure at the interface may stabilize the liquid metal layer against drop ejection. In general it should be stressed that for negligible pressure difference between the reservoir and plasma a static arrangement is difficult to be established. Finally, the pores size and the number of them do not affect the static configuration of the liquid metal. They will play a significant role and may prevent the static configuration from being established, when the dynamic flow configuration is considered.

3 CAPILLARY FLUID MOTION WITHIN A PORE

3.1 Modelling and Numerical Methodology

As a first attempt to provide an upper bound of the convective effects within the CPS matrix, the flow within a cylindrical pore is examined. This simplified geometry overestimates the permeability of the CPS but provides the framework for studying the interplay between the different forces that act towards pushing liquid lithium out of the porous matrix or resist its motion. Emphasis is placed in studying the potential of the CPS system to act as a capillary pump against gravity, viscosity and magnetic braking. A quasi steady state configuration is examined where the time evolution of the interface shape, f, is captured via the kinematic condition while the velocity and pressure fields are concurrently updated neglecting transients. The volumetric flow rate of liquid lithium is obtained, along with the meniscus shape at the interface, for known interfacial tension and contact angle, known pressure drop and material properties. In the present study the hydrodynamic problem is examined in the context of axisymmetry in order to obtain an understanding of the operation principle of the capillary pump. As a next step, a radial magnetic field will be introduced in order to assess the importance of magnetic damping.

The dimensionless governing equations of the hydrodynamic problem are the continuity equation:

$$\frac{1}{r}\frac{\partial}{\partial r}\left(ru_r\right)+\frac{\partial u_z}{\partial z}=0 \tag{7}$$

the momentum balance:

$$We\mathbf{u}\nabla\mathbf{u}=-\nabla p+Ca\nabla\cdot\underline{\underline{\tau}}_v-Bo\mathbf{e}_z \tag{8}$$

where: $\hat{u}=\frac{\sigma R_0}{\mu h_0}$ is the characteristic velocity and $Bo=\frac{\rho g R_0^2}{\sigma}, We=\frac{\rho\hat{u}^2 R_0}{\sigma}, Ca=\frac{\mu\hat{u}}{\sigma}$ are the dimensionless Bond, Webber and Capillary numbers, respectively, that relate the gravitational, inertial and viscous forces, with surface tension. Furthermore the kinematic condition on the interface reads:

$$u_r \frac{\partial f}{\partial r} = u_z, \quad z = f(r) \tag{9}$$

while the normal stress balance is:

$$\left(p_{in} \underline{\underline{I}} - Ca \underline{\underline{\tau}}_v \right) \cdot \mathbf{n} - p_{out} \underline{\underline{I}} \cdot \vec{n} = -2H\vec{n} = -\left(\frac{\partial \mathbf{t}}{\partial s} - \frac{\mathbf{n}}{R_2} \right) \qquad z = f(r) \tag{10}$$

The pressure in the reservoir is set to p_{in} whereas the pressure drop, p_{in}-p_{out}, is determined by the static arrangement. Symmetry conditions prevail at the axis of symmetry,

$$v(r=0,z)=0, \quad \partial u / \partial r(r=0,z)=0 \tag{11}$$

Finally the transverse velocity is set to zero at the pore entrance, v(z=0,r)=0, whereas at the pore wall a slip length, ℓ, is allowed near the meniscus tip in order to accommodate the rise velocity of the liquid metal

$$v(r=1,z;t)=0, \quad u(r=1,z;t)=\frac{\partial f}{\partial t}(r=1;t)e^{-\frac{1-x}{\varepsilon}}, \quad x=\frac{z}{f(r;t)}, \quad \varepsilon=\frac{\ell}{R_0} \tag{12}$$

The above relationship ensures that the no-slip condition pertaining to the axial velocity at the wall, is reinstated after a very small slip length ℓ. Variable x is introduced in order to fix the size of the mesh in the r, x plane within 0 and 1. In this fashion the shape of the interface is introduced throughout the problem formulation but the process of following changes in the shape of the interface is facilitated [17,18], Figure 6.

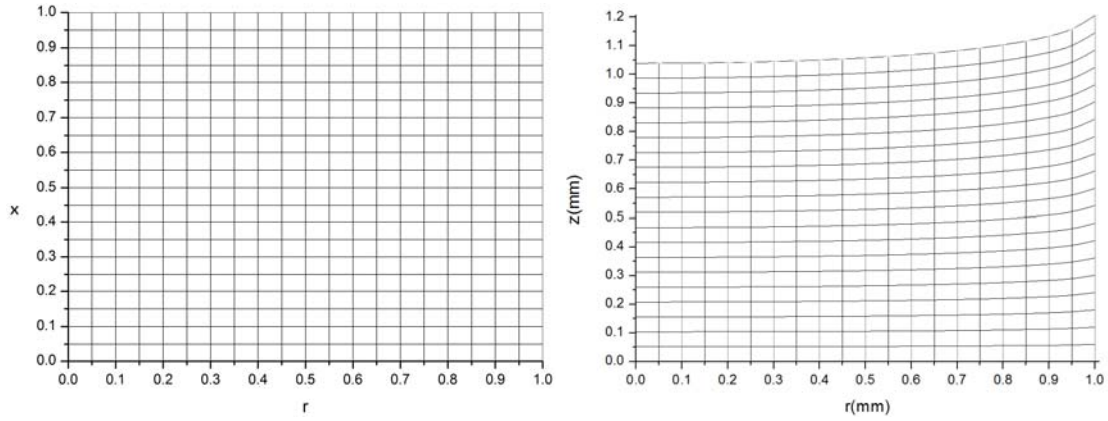

(a) (b)

Figure 6. (a) Computational mesh and (b) real mesh, at the same time instant.

The velocity and pressure fields, (u,v) and p, respectively, along with the shape of the interface f constitute the unknowns of the problem as function of the cylindrical coordinates (r,x=z/h) and time t. The finite element representation is employed for the discretization of the unknowns

$$(u,v)=\sum_{i=1}^{M}\left(u_i(t),v_i(t)\right)\mathrm{X}_i(r,z), \quad P=\sum_{i=1}^{N}P_i(t)\Psi_i(r,z), \quad f(r)=\sum_{i=1}^{K}f_i(t)B_i(r) \tag{13}$$

with the biquadratic, $X_i(r,z)$, and bilinear, $\Psi_i(r,z)$, basis functions for the velocity and pressure field, respectively, in the standard staggered mesh approach. In this fashion the weak form of the momentum equation is obtained:

$$R_{ki} = \iint_{A^e} \left[P\vec{\nabla}\cdot\left(X_i\vec{e}_k\right) - Ca\underline{\underline{\tau}}_v : \vec{\nabla}\left(X_i\vec{e}_k\right) - X_i We\left(\vec{u}\cdot\vec{\nabla}\vec{u}\right)\cdot\vec{e}_k \right] dA -$$

$$\int_{A^e\cap\Gamma_{top}} X_\iota \left[P_{out}\vec{n}\cdot\vec{e}_k - \left(\frac{\partial\vec{t}}{\partial s} - \frac{\vec{n}}{R_2}\right)\cdot\vec{e}_k \right] dS \qquad \text{dynamic condition for meniscus}$$

$$\int_{A^e\cap\Gamma_{Bot}} X_\iota \left[P_{Res}\vec{n}\cdot\vec{e}_k \right] dS \qquad \text{fixed reservoir pressure}$$

(14)

with k=1,2 standing for the z and r components of momentum, along with continuity

$$R_{3i} = \iint_{A^e} \Psi_i \left(\frac{u}{r} + \frac{\partial u}{\partial z} + \frac{\partial v}{\partial r} \right) r dr dz \tag{15}$$

and the kinematic condition

$$R_{4i} = \int_{\Gamma^e} \Phi_i \left[\frac{f^{n+1} - f^n}{\Delta t} - u^{n+1} + v^{n+1}\frac{\partial f}{\partial r}^{n+1} \right] dS \; ; \tag{16}$$

the latter is discretized in time using a fully implicit scheme. The aforementioned system of equations produces a set of nonlinear equations with a banded Jacobian matrix that is solved using Newton's iterations.

In order to validate the above numerical model the results were tested for the case of a pore with a radius of 1mm that is gradually filled with water from a reservoir held at atmospheric pressure, solely via capillary forces, until a static arrangement within the pore is established. Fig. 7a provides a sequence of shapes for the meniscus during the process of capillary rise. As can be gleaned from the final stages of capillary rise, and more clearly in fig.7b, the meniscus shape, obtained with and without inertial effects, is in good agreement with the static arrangement of liquid water within a cylindrical pore with a radius of 1 mm obtained independently via solution of the Young Laplace equation at static equilibrium, i.e. eq. (10) without the viscous terms.

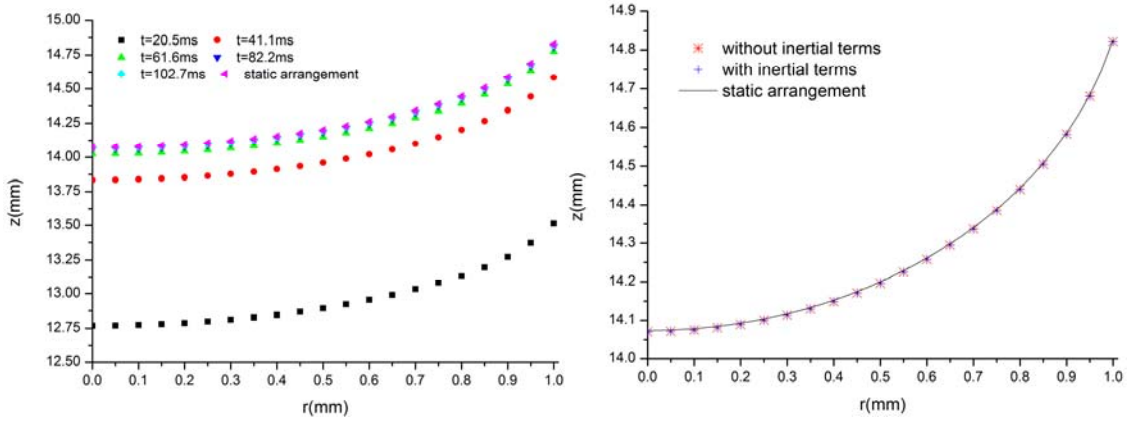

(a) (b)

Figure 7. (a) Time evolution of the meniscus shapes during the process of capillary rise and (b) Comparison of the current numerical model (with and without inertial terms) against the static arrangement of liquid water within a pore.

3.2 Results and Conclusions

Currently the above methodology is employed in order to assess how the pore radius affects the seepage velocity of liquid lithium within a pore of 1mm in height. Upon decreasing the pore radius the capillary rise velocity is seen to decrease linearly owing to the emergence of viscous effects along the radial direction, fig. 8a. This scaling qualitatively agrees with the viscous scale employed for making velocity dimensionless. It corresponds with a balance between the axial pressure drop generated due to capillary wetting of the interface and radial momentum diffusion via viscosity

$$\mu \frac{\partial^2 u}{\partial r^2} = -\frac{\partial P}{\partial z} \Rightarrow \frac{\mu \hat{u}}{R_0^2} \sim \frac{\sigma / R_0}{h_0} \Rightarrow \hat{u} \sim \frac{\sigma R_0}{\mu h_0} \tag{17}$$

It should be stressed that contrary to the case shown in figure 7 the flow arrangement with lithium rising shown in Figure 8 is far from static equilibrium hence the rise velocity is relatively large while being slowly reduced as the height of the column increases. Nevertheless, for relatively large pore sizes, R_0~0.1 mm, the simulations with inertia effects tend to reduce the seepage velocity in comparison with the simulation assuming purely Stokes flow. Consequently, the time needed for the liquid metal to exit the pore tents to be bigger for the case where the inertial terms are taken into account, fig. 8b. In this context the importance of transient effects at the pore level seems to play a role at relatively large pore sizes and this is currently under numerical investigation in order to be validated.

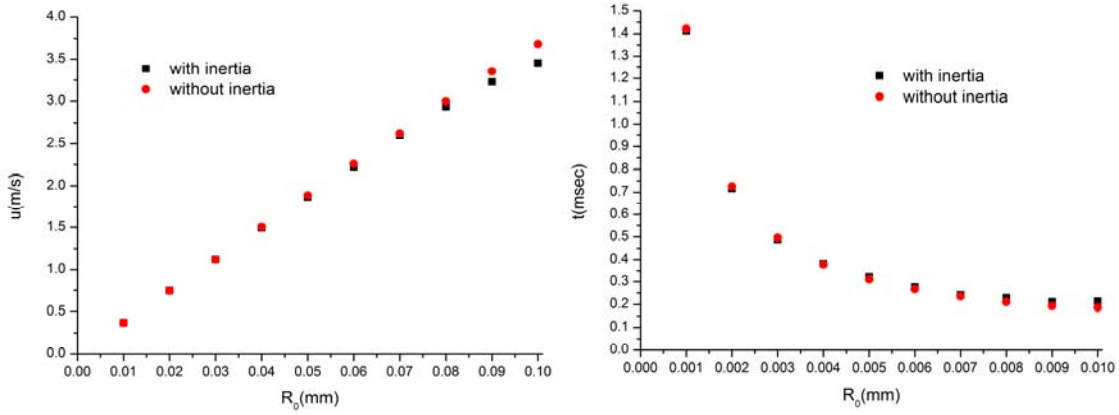

(a) (b)

Figure 8. (a) Seepage velocity at the exit of the pore and (b) Time needed for the liquid metal to exit the pore as a function of the pore radius both with and without the inertial terms included

As a next step, a radial magnetic field will be introduced in order to assess the importance of magnetic damping. Coupling with charge conservation will be performed in order to obtain the electric potential and through it the Lorentz force. Emerging axial electric potential gradients will generate a rotationally symmetric flow pattern that entails flow in the azimuthal direction. This type of interaction, in the presence of thermal effects, will generate a microscopic thermoelectric effect [19] which, however, is expected to be subdominant to that due to surface tension. Such calculations will offer the opportunity to test this assertion by incorporating the results of the analysis regarding the thermoelectric effect on the hydrodynamic analysis on the level of a single pore.

AKNOWLEDGEMENTS

This work is supported by (a) the National Programme for the Controlled Thermonuclear Fusion, Hellenic Republic, (b) the EJP Cofund Action SEP-210130335 EUROfusion.

REFERENCES

[1] Christofilos, N.C., (1989), "Design for a high power-density Astron reactor", *Journal of Fusion Energy*, Vol. 8, Issue 1/2, pp. 97-105.

[2] Mirnov, S.V., Dem`yanenko, V.N., Muravev, E.V., (1992), "Liquid metal divertors", *Journal of Nuclear Materials*, Vol. 196-198, pp. 45-49.

[3] Ying, A.V. , Morley, N., Smolentsev, S., Gulec, K., Fogarty, P. (2000), "Free surface heat transfer and innovative designs for thin and thick liquid walls", *Journal of Fusion Engineering & Design*, Vol. 49-50, pp. 397-406.

[4] Mirnov, S.V., Azizov, E.A., Evtikhin, V.A., Lazarev, V.B., Lyublinski, I.E., Vertkov, A.V., Prokhorov, D. Yu., (2006), "Experiments with lithium limiter on T-11M tokamak and applications of the lithium capillary-pore system in future fusion reactor devices", *Journal of Plasma Physics and Controlled*, Vol. 48, pp. 821-837.

[5] Mirnov, S.V., Evtikhin, V.A, (2006), "The tests of liquid metals (Ga, Li) as plasma facing components in T-3M and T-11M tokamaks", *Journal of Fusion Engineering & Design*, Vol. 81, pp. 113-119.

[6] Gomes, R.B., Fernandes, H., Silva, C., Sarakovskis, A., Pereira T., Figueiredo, J., et al., (2008), "Interaction of a liquid gallium jet with the tokamak ISTTOK edge plasma", *Journal of Nuclear Materials*, Vol. 415, Issue 1, pp. S989–S992.

[7] Gomes, R.B., Silva, C., Fernandes, H., Duarte, P., Nedzelskiy, I., Lielausis, O., et al., (2011), "ISTTOK tokamak plasmas influence on a liquid gallium jet dynamic behavior", *Journal of Fusion Engineering & Design,* Vol. 83, pp. 102-111.

[8] Pelekasis, N.A., Benos, L.Th., Gomes, R.B., (2014), "Deflection of a liquid metal jet/drop in a tokamak environment", *Journal of Fusion Engineering & Design*, Vol. 89, pp. 2930-2936.

[9] Morley, N.B., Abdou, M.A., Anderson, M., Calderoni, P., Kurtz, R.J., Nygren, R., et al., (2006), "Overview of fusion nuclear technology in the US", *Journal of Fusion Engineering & Design*, Vol. 81, pp. 33-43.

[10] Golubchikov, L.G., Evtikhin, V.A, Lyublinski, I.E., Pistunovich, V.I., Potapov, I.N., Chumanov, A.N., (1996), "Development of a liquid-metal fusion reactor divertor with a capillary-pore system", *Journal of Nuclear Materials*, Vol. 233-237, pp. 667-672.

[11]Evtikhin, V.A, Vertkov, A.V., Lyublinski, I.E., Khripunov, B.I., Petrov, V.B., Mirnov, S.V., (2002), "Research of lithium capillary-pore systems for fusion reactor plasma facing components", Journal of Nuclear Materials, Vol. 307-311, pp. 1664–1669.

[12] Piet, S.J, Jeppson, D.W, Muhlestein, L.D., Kazimi, M.S. & Corradini M.L. (1987) Liquid metal chemical reaction safety in fusion facilities, Fusion Engineering & Design 5 273-298.

[13] G. Mazitelli, M.L. Apicella, M. Marinucci, C. Mazzotta, V. Pericoli Ridolfini, O. Tudisco, et al., 21st IAEA fusion energy conference, Chengdu, China, 2006, ex/p4–6.

[14]M. J. Miksis, (1981) Shape of a drop in an electric field, Phys. Fluids 24(11), 1967-1972.

[15] Dubash, N., Mestel, A.J. (2007), "Behaviour of a conducting drop in a highly viscous fluid subject to an electric field", *Journal of Fluid Mechanics*, Vol. 581, pp. 469–493.

[16] Taylor, G. I. 1966a The force exerted by an electric field on a long cylindrical conductor. Proc. R. Soc. Lond. A 291, 145–158.

[17] S. F. Kistler and L. E. Scriven 1984, Coating flow theory by finite element and asymptotic analysis of the Navier-Stokes system, Int. J for Num. Meth. Fluids, vol. 4, 207-229.

[18] E. Widjaja, Nai-Chi Liu, M. Li, R. T. Collins, O. A. Basaran, M. T. Harris, Dynamics of sessile droplet evaporation: A comparison of the spine and the elliptic mesh generation methods, Computers and Chemical Engineering 31 (2007) 219–232

[19]Kaldre, I., Lielausis, O. (2014), "Role of thermoelectromagnetic forces in capillary porous systems proposed for liquid metal cooling of fusion reactor components, *9th International Pamir conference on fundamental and applied MHD*, Riga, Latvia, 16-20 June 2014.